The EMBO Journal (2009) 28, 466–476 | © 2009 European Molecular Biology Organization | All Rights Reserved 0261-4189/09
www.embojournal.org

THE EMBO JOURNAL

Accumulation of raft lipids in T-cell plasma membrane domains engaged in TCR signalling

Tobias Zech[1,5,6], Christer S Ejsing[2,6], Katharina Gaus[3,4], Ben de Wet[1], Andrej Shevchenko[2], Kai Simons[2] and Thomas Harder[1,*]

[1]Sir William Dunn School of Pathology, University of Oxford, Oxford, UK, [2]Max Planck Institute of Molecular Cell Biology and Genetics, Dresden, Germany, [3]Centre for Vascular Research, University of New South Wales, New South Wales, Australia and [4]Department of Haematology, Prince of Wales Hospital, Sydney, New South Wales, Australia

Activating stimuli for T lymphocytes are transmitted through plasma membrane domains that form at T-cell antigen receptor (TCR) signalling foci. Here, we determined the molecular lipid composition of immunoisolated TCR activation domains. We observed that they accumulate cholesterol, sphingomyelin and saturated phosphatidylcholine species as compared with control plasma membrane fragments. This provides, for the first time, direct evidence that TCR activation domains comprise a distinct molecular lipid composition reminiscent of liquid-ordered raft phases in model membranes. Interestingly, TCR activation domains were also enriched in plasmenyl phosphatidylethanolamine and phosphatidylserine. Modulating the T-cell lipidome with polyunsaturated fatty acids impaired the plasma membrane condensation at TCR signalling foci and resulted in a perturbed molecular lipid composition. These results correlate the accumulation of specific molecular lipid species with the specific plasma membrane condensation at sites of TCR activation and with early TCR activation responses.

The EMBO Journal (2009) **28,** 466–476. doi:10.1038/emboj.2009.6; Published online 29 January 2009
Subject Categories: membranes & transport; signal transduction
Keywords: lipid rafts; plasma membrane domains; quantitative shotgun lipidomics; TCR signalling

Introduction

T lymphocytes are activated upon conjugation with cognate antigen-presenting cells. Multiple receptor–ligand interactions at the contact zone between these cells, the immunological synapse, determine the outcome of this encounter (Huppa and Davis, 2003). The key activation signal is provided by the T-cell antigen receptor (TCR) upon ligation with a cognate peptide—major histocompatibility complex expressed on the surface of the antigen-presenting cell. The TCR signals are relayed to the T-cell interior by signalling protein complexes, which assemble in the T-cell plasma membrane (Harder, 2004).

Numerous proteins have been identified that drive the formation and sustain TCR signalling assemblies. Cytosolic signalling enzymes and adaptor proteins, such as PLCγ and Grb2, interact with the transmembrane protein linker for activation of T cells (LAT), and subunits of the TCR complex (Chan *et al*, 1992; Zhang *et al*, 1998; Harder and Kuhn, 2000). Single-molecule microscopy showed that activation of the TCR induces the formation of membrane domains that are built by a network of protein–protein interactions that exclude or trap specific signalling proteins (Douglass and Vale, 2005; Suzuki *et al*, 2007a).

Plasma membrane domains engaged in TCR signal transduction have been ascribed the properties of lipid rafts that entail the functional segregation of cholesterol, sphingolipids and saturated glycerophospholipids. On the basis of model membrane studies, lipid rafts are proposed to adopt a condensed liquid-ordered (Lo) state that coexist with a non-raft liquid-disordered bilayer (Brown and London, 1997; Veatch and Keller, 2003; Simons and Vaz, 2004). In the Lo phase, the planar cholesterol ring systems align with saturated fatty acid moieties of phosphatidylcholine (PC) and sphingomyelin (SM). From this biophysical perspective, the concept of raft domains at TCR signalling sites has received experimental support: Laurdan 2-photon fluorescence microscopy showed that T-cell plasma membrane domains engaged in TCR activation are more condensed as compared to other plasma membrane regions (Gaus *et al*, 2005).

Although the raft concept of membrane organization has been subject to controversy (Munro, 2003; Shaw, 2006), the model is now gaining increased acceptance through studies applying novel methodologies. At present, lipid rafts are considered to be dynamic, nanometer-sized sterol-, sphingolipid-, saturated glycerophospholipid-enriched membrane domains (Hancock, 2006). These metastable membrane assemblies can be stabilized locally by lipid–lipid and lipid–protein interactions to coalesce and form functional domains for cell surface receptor signal transduction (Simons and Toomre, 2000). Indeed, image analyses and single molecule tracking showed accumulation or the confinement of cytosolic fatty acid-anchored raft markers at T-cell activation domains (Ike *et al*, 2003; Tavano *et al*, 2006). However, direct evidence for an accumulation of distinct molecular lipid species, which support the formation of ordered membrane phases at TCR signalling plasma membrane domains is lacking, and thus the issue of lipid raft coalescence at TCR activation sites remains disputed (Munro, 2003; Shaw, 2006).

*Corresponding author. Sir William Dunn School of Pathology, University of Oxford, South Parks Road, Oxford OX1 3RE, UK.
Tel.: +44 1865 285 690; Fax: +44 1865 275 501;
E-mail: thomas.harder@path.ox.ac.uk
[5]Present address: The Beatson Institute for Cancer Research, Glasgow, UK
[6]These authors contributed equally to this work

Received: 18 December 2008; accepted: 7 January 2009; published online: 29 January 2009

Here, we have taken a direct approach to investigate whether TCR activation domains in the plasma membrane exhibit a characteristic molecular lipid composition. To this end, we have performed a global analysis of the molecular lipid composition of immunoisolated native TCR activation domains by mass spectrometry and compared it with control plasma membrane fragments enriched in transferrin receptors (TfRs). We provide, for the first time, direct evidence for the functional segregation of cholesterol, SM and distinct glycerophospholipid species at TCR activation domains, thereby emphasizing the importance of the lipid composition for defining these plasma membrane domains.

Results

Distinctive plasma membrane fractions prepared by immunoisolations

We used an established immunoisolation procedure for isolating native T-cell plasma membrane fragments harbouring the TCR activation machinery (Harder and Kuhn, 2001). Magnetic beads coated with TCR-activating αCD3 antibodies were conjugated at 0°C to Jurkat cells and activation occurred upon shift to 37°C for 3 and 10 min. The bead–cell conjugates were mechanically homogenized by nitrogen cavitation. The plasma membrane fragments bound to the magnetic beads were isolated and subjected to western blot analysis and quantitative mass spectrometric lipid analysis. Considering the specific and time-dependent concentration of TCR signalling protein assemblies in the αCD3 immunoisolates, they can be taken as surrogates of TCR activation plasma membrane domains (Harder and Kuhn, 2000, 2001). As a comparative control, we established a similar αTfR immunoisolation of Jurkat plasma membrane fragments that are enriched in TfRs but devoid of TCR signalling machinery (Harder and Kuhn, 2000).

To establish the use of the immunoisolation methodology for the characterization and comparison of the molecular lipid composition of the distinct immunoisolated plasma membrane domains, we sought to determine the relative contamination with intracellular compartments: The amounts of different membrane markers in αCD3 and αTfR immunoisolates were measured using the LICOR Odysee^{TM} western blot system, which allows quantification of the signal strength of the immunoreactive bands. Immunoisolates were prepared from 5×10^7 Jurkat cells and the western blot signal strengths were related to those of a lysate of 1.25×10^5 Jurkat cells corresponding to 0.25% of the Jurkat starting material (Figure 1A). As reported earlier, LAT plasma membrane adaptor protein was concentrated in αCD3 immunoisolated Jurkat plasma membrane domains—reflecting the assembly of TCR signalling machinery—and TfRs were accumulated in the αTfR immunoisolates (Harder and Kuhn, 2000).

In line with this previous analysis, LAT was also recovered in αTfR immunoisolates following 37°C incubation at approximately 10- to 15-fold higher amounts than in 0.25% of Jurkat cell starting material (Figure 1A). Inactive LAT resides in the plasma membrane of resting Jurkat cells. Therefore, this value indicated a slightly higher plasma membrane recovery in αTfR immunoisolates than the previously estimated 1–2% recovery of Jurkat cell surface in both immunoisolates (Harder and Kuhn, 2000). Vice versa, TfR was recovered in αCD3 immunoisolates, even though this occurred at a lower fraction relative to the total cellular pool than for the LAT in αTfR immunoisolates (Figure 1A). This may reflect the loss of the intracellular endosomal TfR pool in the αCD3 immunoisolates and a depletion of TfRs from plasma membrane domains engaged in TCR signalling.

We next verified that αCD3 and αTfR immunoisolates indeed contained minor and similar amounts of intracellular membranes. We determined the recovery of ER membrane and mitochondria in the immunoisolates by these western blots using the respective calnexin and MTCO1 markers. The results allowed us to conclude that upon 37°C incubations the amount of ER and mitochondrial markers recovered in the immunoisolates was less than 0.04% of the total (Figure 1A). The immunoisolates thus strongly depleted these intracellular membrane compartments relative to plasma membrane that was recovered in the range of 1–2% of the whole plasma membrane (Harder and Kuhn, 2000). This analysis also showed that the contents of these minor contaminations were similar in both immunoisolates. Additional western blot analyses showed a strong signal for the ER marker sec61 and the endosomal GTPase Rab7 in the Jurkat cell lysate, although they were barely detectable in the αTfR and αCD3 immunoisolates prepared from 200-fold higher number of Jurkat cells (Supplementary Figure S1). The TCR signalling machinery accumulation, TfR concentration and the relative homogeneity of plasma membrane fragments in the immunoisolates were routinely verified by such western blots before they were subjected to an analysis of their lipidome.

We monitored the recovery of membrane lipids in the αCD3 and αTfR immunoisolates. We quantified the amount of PC and SM recovered in lipid extracts of the immunoisolates by precursor ion scanning (PIS) for the characteristic phosphorylcholine fragment ion with *m/z* 184.1 (Figure 1B). Both αCD3 and αTfR immunoisolates showed a time-dependent increase in the yield of PC and SM that after 3 to 10 min was equal to 0.1–0.3% of the PC extracted from an equivalent number of Jurkat cells (Figure 1B). The highest amount of PC recovered in control experiments, in which magnetic beads were coated with an IgG antibody and incubated with Jurkat cells for 10 min, never exceeded 20% of the PC recovered in αCD3 immunoisolates (data not shown).

In summary, the immunoisolation procedure produced two distinct plasma membrane fragments with different protein composition, similarly depleted of proteins and lipids from intracellular compartments, and with similar kinetics of lipid recovery. It should be noted that αCD3 immunoisolates contained a fraction of non-signalling plasma membrane as indicated by the presence of some TfR (Figure 1A).

To characterize the molecular lipid composition of the immunoisolated plasma membrane fragments, we used mass spectrometric methodology developed for comprehensive and quantitative characterization of membrane lipidomes (Ejsing *et al*, 2006). The αCD3, αTfR immunoisolates and Jurkat cells were spiked with internal lipid standards and subjected to lipid extraction. PC and SM species were determined by PIS *m/z* 184.1 analysis (Ekroos *et al*, 2002; Liebisch *et al*, 2004). Molecular diacylglycerol (DAG), phosphatidic acid (PA), phosphatidylglycerol (PG), phosphatidylethanolamine (PE), phosphatidylserine (PS) and phosphatidylinositol (PI) species were determined by quantitative multiple PIS (Ejsing *et al*, 2006). Multiple reaction monitoring was used

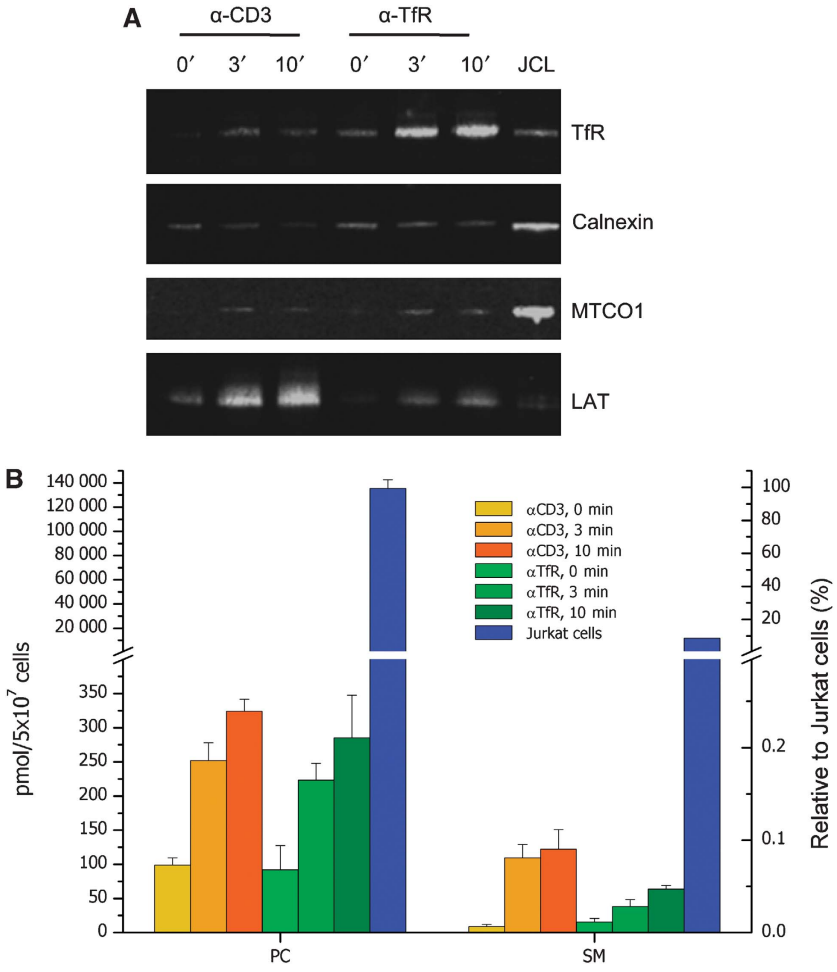

Figure 1 (**A**) Relative recovery of LAT, TfR, the ER membrane marker calnexin and the mitochondrial marker cytochrome c oxidase complex 1 (MTCO1) in αCD3 and αTfR immunoisolated plasma membrane fragments. The proteins of the respective Jurkat cell fractions were analysed using the LICOR Odysee™ western blot system, which allows an assessment of the relative strengths of western blot signals. The signals from the same immunoisolate preparations using 5×10^7 Jurkat cells were related to the signal strength from cell lysates from 1.25×10^5 Jurkat cells (JCL, corresponding to 0.25% of the number of cells used for the immunoisolations). These blots showed that in both immunoisolates the ER and mitochondrial markers were depleted at least 5-fold over the plasma membrane-associated LAT and TfR following 3 min and 10 min of 37°C incubation of the bead–cell conjugates. There is no selective contamination of ER and mitochondria in the immunoisolates. (**B**) Recovery of Jurkat lipid membrane estimated by the total amount of PC and SM extracted from immunoisolates. PC and SM species were quantified by a PIS *m/z* 184.1 analysis using internal standards as outlined in Materials and methods. The total amount of PC and SM was calculated as the sum of individual species from the respective lipid class. The recovery of PC and SM increased progressively with the time of incubation of the bead–cell conjugates at 37°C. On the right ordinate, the lipid yields are depicted as molar percentage of the PC in total Jurkat cells ($n = 3$ independent experiments, average estimate ± s.d.).

for the analysis of ceramide (Cer), hexosylceramide (HexCer), diosylceramide (Hex2Cer) species and cholesterol (Ejsing *et al*, 2006; Liebisch *et al*, 2006).

Accumulation of SM, cholesterol and saturated PC species in αCD3 immunoisolates

The analysis for PC and SM species provided the first evidence that TCR activation domains comprise a distinctive molecular lipid composition (Supplementary Figure S2). αCD3 immunoisolates obtained after 3 and 10 minutes showed a pronounced enrichment of SM species (SM 34:1;2, *m/z* 703.6, being the most abundant species) in comparison with αTfR immunoisolated plasma membrane fragments and Jurkat cells (Figure 2A and Supplementary Figure S3). Furthermore, quantitative profiling showed that the αCD3 immunoisolates were systematically enriched in PC species with saturated fatty acid moieties and depleted in PC species having multiple double bonds (Figure 2B). In comparison, the proportion of saturated PC species decreased from 30% in the αCD3 immunoisolates to 20% in the αTfR immunoisolates and to 15% in Jurkat cells. The distinctive PC and SM species composition of the αCD3 immunoisolates was achieved following 3 min incubation of the bead–cell conjugates (Supplementary Figure S2A and B). In comparison with αTfR immunoisolates and Jurkat cells, the amount of PC species having 36 or more carbon atoms was reduced in the αCD3 immunoisolates, whereas the amount of PC species having 32 carbon atoms was concomitantly increased (Figure 2C).

We further characterized the lipidome of TCR activation plasma membrane domain by comparing the lipid class composition of αCD3 and αTfR immunoisolates (Figure 3).

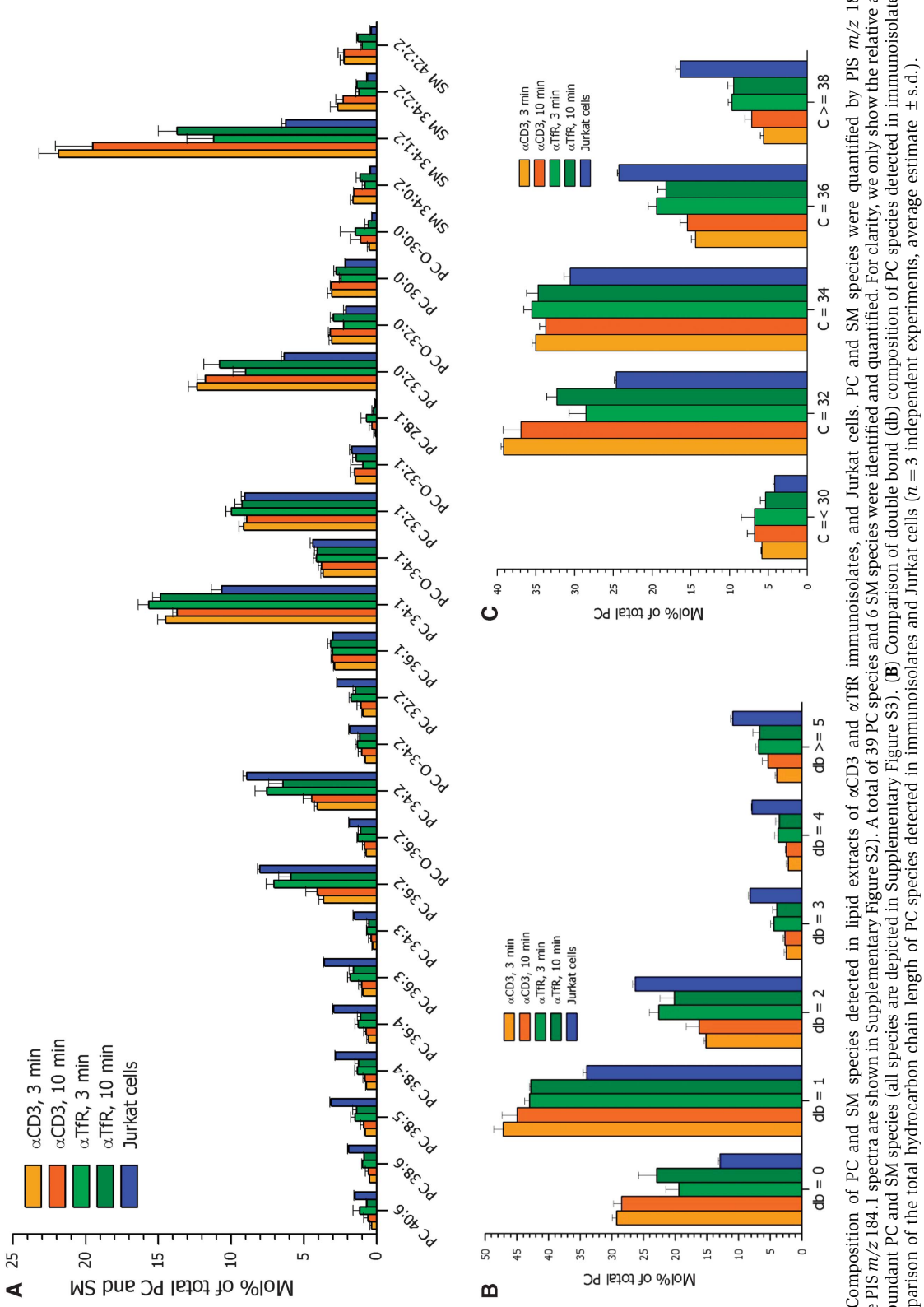

Figure 2 (**A**) Composition of PC and SM species detected in lipid extracts of αCD3 and αTfR immunoisolates, and Jurkat cells. PC and SM species were quantified by PIS *m/z* 184.1 analysis (representative PIS *m/z* 184.1 spectra are shown in Supplementary Figure S2). A total of 39 PC species and 6 SM species were identified and quantified. For clarity, we only show the relative abundance of the 26 most abundant PC and SM species (all species are depicted in Supplementary Figure S3). (**B**) Comparison of double bond (db) composition of PC species detected in immunoisolates and Jurkat cells. (**C**) Comparison of the total hydrocarbon chain length of PC species detected in immunoisolates and Jurkat cells ($n = 3$ independent experiments, average estimate ± s.d.).

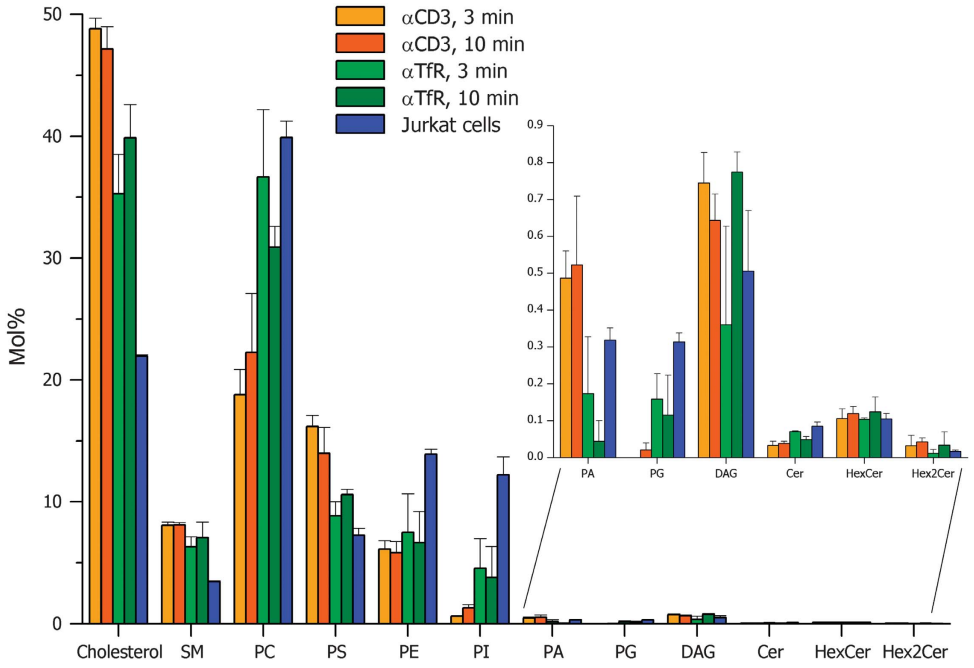

Figure 3 Lipid class composition of 3 and 10 min 37°C immunoisolates, and Jurkat cells. The 3 and 10 min αCD3 immunoisolates show a distinct lipid class composition with a higher concentration of cholesterol and PS, and a notable reduction of PI and PC in comparison with the αTfR immunoisolates. No conclusions were made on differences between low abundant lipid classes (<1 mol%, inset). The mass spectrometric lipid analysis allowed the identification and quantification of 101 distinct lipid species. The mol% of lipid classes was calculated as the sum of the mol% of all detected lipid species of the respective lipid class. The inset shows the composition of low abundant lipid classes. PA, DAG, PG, Cer, HexCer and Hex2Cer species were detected at low levels in all repetitions of the experiment ($n = 3$ independent experiments, average estimate ± s.d.).

Following 3 and 10 min, both αCD3 and αTfR immunoisolates were enriched in cholesterol and SM as compared with Jurkat cells (Figure 3). In comparison, the cholesterol content was ~1.3-fold higher in αCD3 immunoisolates as compared with αTfR immunoisolates. These results show that the composition of TCR activation domains is distinctive and characterized by increased content of cholesterol (Figure 3), SM and saturated PC species, although PC species having multiple double bonds are depleted (Figure 2).

A characteristic composition of PS, PI and PE species in αCD3-immunoisolated TCR signalling domains

Next we evaluated the composition of glycerophospholipid PS, PI and PE species believed to predominantly reside in the cytoplasmic membrane leaflet (Figure 4A) (Zachowski, 1993; van Meer *et al*, 2008). We observed that in αCD3 immunoisolates, the content of PS was ~1.5-fold higher, whereas the content of PI was ~3-fold lower as compared with αTfR immunoisolates. The abundance of PE was similar in both immunoisolates (Figures 3 and 4A); however, the αCD3 immunoisolates exhibited an increased fraction of plasmenyl PE species having a vinyl-ether-linked hydrocarbon moiety at the *sn*-1 position (Figure 4B, Supplementary Figure S4A).

The fatty-acid composition of PS, PE and PI species of Jurkat cells, αCD3 and αTfR immunoisolates was markedly different as compared with that of the PC species. Whereas a sizable fraction of PC species comprised only saturated fatty-acid moieties (e.g., PC 32:0; Figure 2), we only detected PE, PS and PI species having at least one double bond (Figure 4A). Furthermore, we did not observe an enrichment of PE, PS and PI species having more saturated fatty acid moieties in the αCD3 immunoisolates as compared with αTfR immunoisolates and Jurkat cells. We note, however, that the enrichment of PS in αCD3 immunoisolates was primarily attributed to the mono-unsaturated species PS 18:0–18:1.

Some lipids were detected at less than 1 mol% (Figure 3). Of these lipids, PA and DAG are generated by cytoplasmic signalling reactions that have been shown to occur at T-cell activation sites (Figure 3 (Spitaler *et al*, 2006; Mor *et al*, 2007)). The relative abundance of these low abundant lipids did not show major differences between the immunoisolates, and minor fluctuations observed were omitted from a detailed interpretation.

Impairment of membrane condensation at TCR activation domains after incorporation of polyunsaturated fatty acids

It was shown previously that polyunsaturated fatty acids attenuate T-cell responses and promote immunosuppressive effects when provided with the diet (Stulnig *et al*, 1998; Shaikh and Edidin, 2006). Thus, to gain further insights into the functional importance of the distinct molecular lipid composition of TCR activation domains, we modulated the Jurkat cell lipidome by incorporating the polyunsaturated eicasopentanoic fatty acid (C20:5). Using Laurdan 2-photon fluorescence microscopy (Gaus *et al*, 2005, 2006), we found that C20:5 treatment impaired membrane condensation at TCR activation sites (Figure 5). The TCR activation sites of C20:5-treated Jurkat cells showed a shift in Laurdan fluorescence emission yielding a lower generalised polarization (GP)

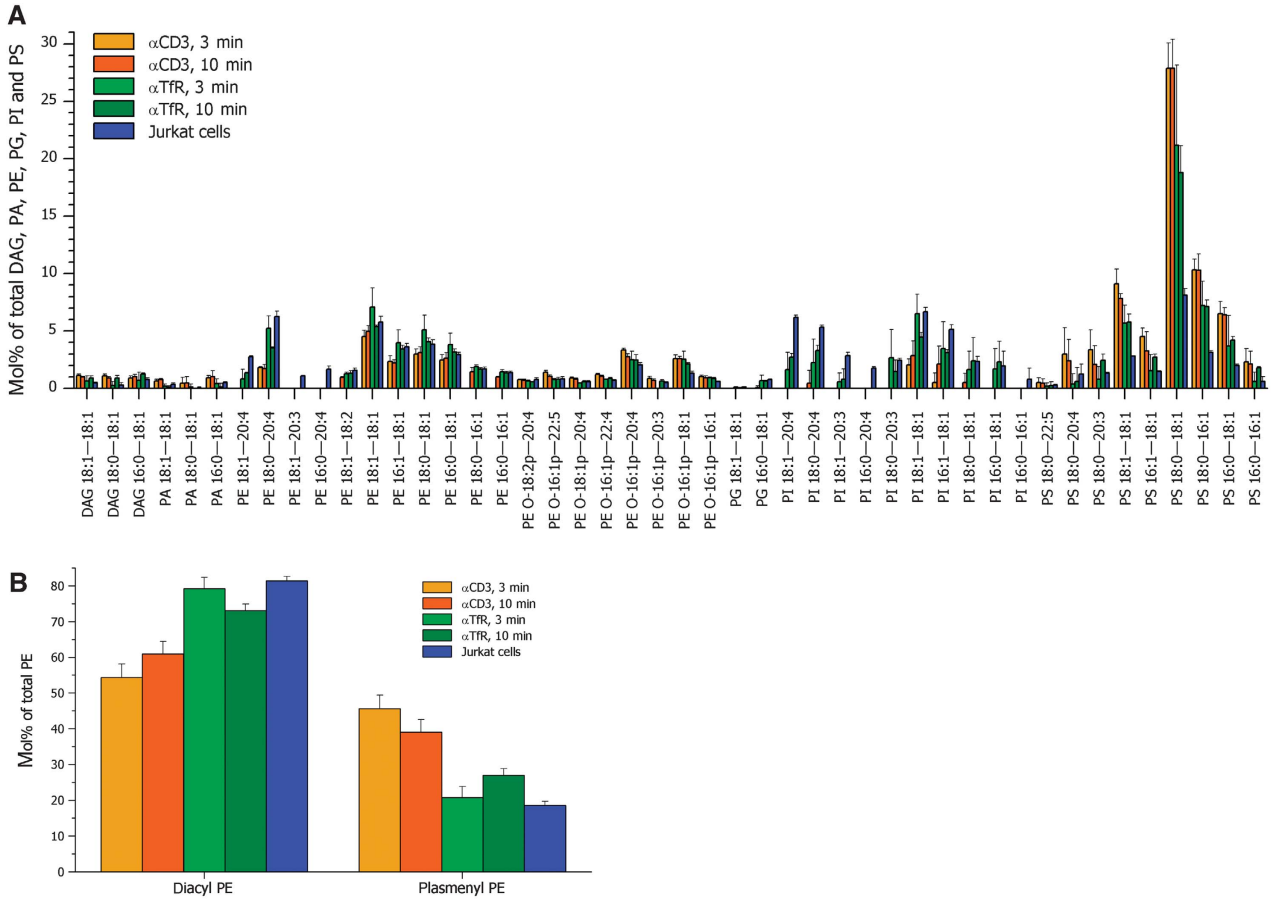

Figure 4 (**A**) Relative abundance of molecular PE, PS, PG, PI, PA and DAG species detected by quantitative multiple PIS analysis of lipid extract of αCD3 and αTfR immunoisolates, and Jurkat cells. (**B**) Profile of diacyl and plasmenyl PE species in immunoisolates and Jurkat cells. The proportion of diacyl and plasmenyl PE species was calculated as the sum of the mol% of PE species of the respective lipid subclass ($n=3$ independent experiments, average estimate ± s.d.).

values as compared with non-treated control cells (Figure 5A and B) and αTfR antibody-coated beads did not show a significant difference in membrane condensation following incorporation of C20:5 (Figure 5D). The impairment of membrane condensation at TCR activation sites after the incorporation of C20:5 is in line with previous findings (Stulnig *et al*, 1998).

Alterations in the lipidome of Jurkat cells after incorporation of C20:5

Next we determined how the incorporation of C20:5 modulated the molecular lipid composition of the Jurkat cells, αCD3 and αTfR immunoisolates. First, the lipidome of C20:5-treated Jurkat cells exhibited an increased content of glycerophospholipid species, including PC species, having polyunsaturated (db⩾5) fatty-acid moieties (Figure 5E, Supplementary Figure S5). We observed that the increased abundance of polyunsaturated PC species was offset by a reduction of PC species with one, two or three double bonds, but not by fully saturated PC species. In addition, we noticed that C20:5-treated Jurkat cells synthesised more SM, in particular the fully saturated species SM 34:0;2 that interact more favourably with cholesterol as compared with SM 34:1;2 (Kuikka *et al*, 2001). We also observed that Jurkat cells mediated a pronounced elongation of C20:5 to C22:5 for subsequent incorporation into PS, PI and PE species. Thus, Jurkat cells modulate their lipidome in response to incorporation of polyunsaturated fatty acids.

The comparative lipidomics analysis of αCD3 and αTfR immunoisolates from Jurkat cells treated with and without C20:5 showed a conserved propensity to segregate cholesterol, SM and saturated PC species at sites of TCR activation (Figure 5E, Supplementary Figure S5). We observed that the lipid class composition of αCD3 immunoisolates from C20:5-treated Jurkat cells resembled that of αCD3 immunoisolates from untreated cells, although with 1.9-fold higher abundance of SM offset by a 1.5-fold reduction of PS. Detailed analysis of the molecular lipid composition of αCD3 immunoisolates from C20:5-treated Jurkat cells showed consistent enrichment of fully saturated PC species, and a pronounced elevation of polyunsaturated PC species offset by the reduction of PC species having one and two double bonds. In addition, we also uncovered that PS and PE species in αCD3 immunoisolates from C20:5-treated Jurkat cells comprised predominantly polyunsaturated (db⩾5) fatty-acid moieties. Thus, we concluded that the overall increase in polyunsaturated lipid species and the perturbations of lipid class composition produced a suboptimal plasma membrane environment that seems to impair the capacity to support membrane condensation, which in turn retards TCR activation.

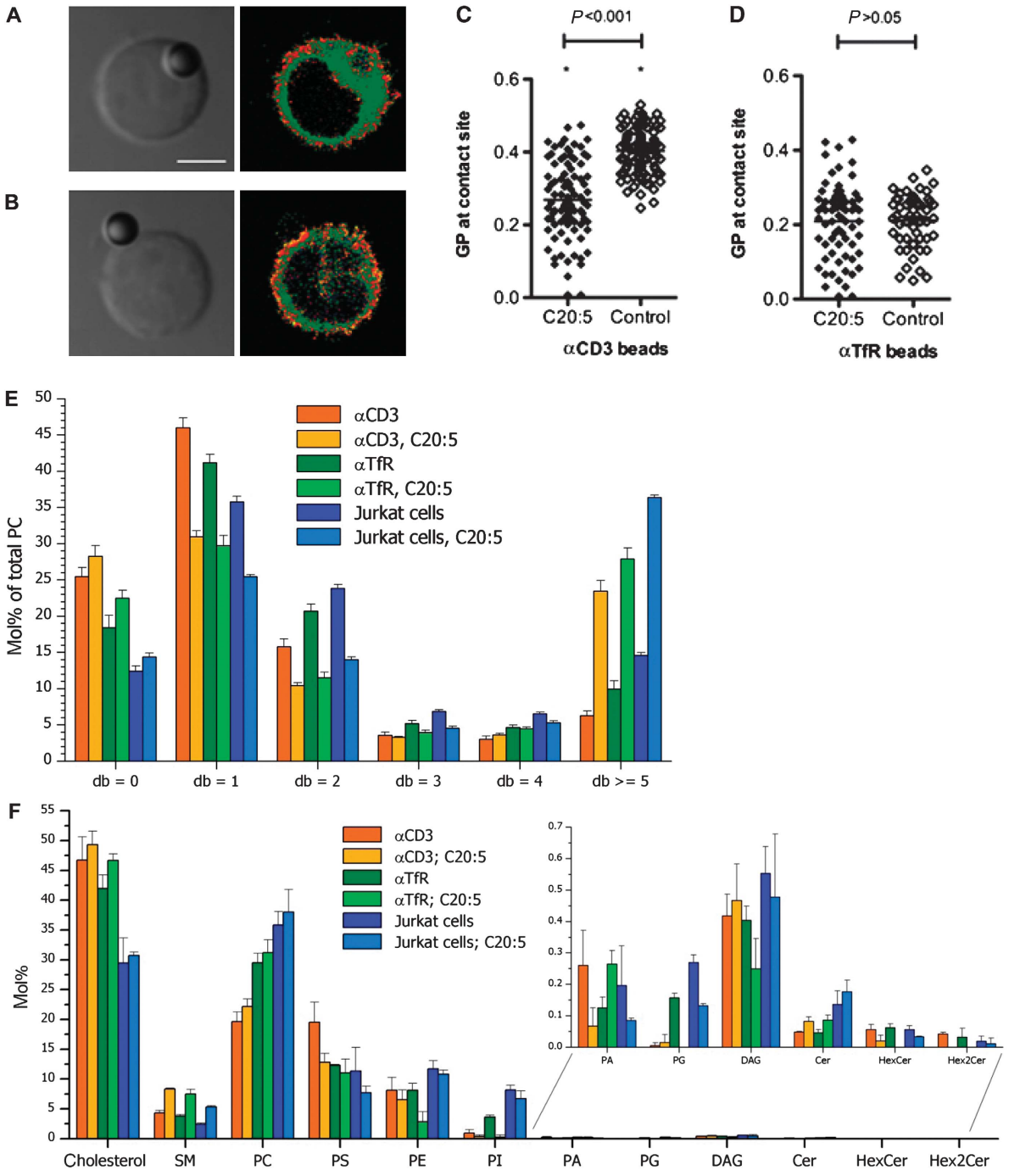

Figure 5 Structure and molecular lipid composition of the plasma membrane at TCR activation domains upon treatment of Jurkat cells with polyunsaturated eicasopentanoic fatty acid. Inhibition of plasma membrane condensation at the TCR activation sites. Laurdan-labelled Jurkat cells (**A**) with and (**B**) without 20:5 polyunsaturated fatty acid eicasopentanoic acid (C20:5) treatment were conjugated with αCD3-coated polystyrene beads for 10 min at 37°C. Cells were adhered and fixed, and Laurdan intensity was imaged simultaneously in two channels (400–460 and 470–530 nm). Intensity images were converted to GP images as described in Materials and methods. For A-B, GP images were pseudo-coloured (GP −0.5 1) and the left panels show corresponding DIC images. Bar = 5 μm. GP values at the bead–cell contact area are plotted for individual conjugates of the Jurkat cells with (**C**) αCD3- and (**D**) αTfR-coated polystyrene beads at 10 min and 37°C. Means are indicated by horizontal lines. For αCD3 bead–Jurkat contact region, the C20:5-treated exhibited significantly lower GP value (◆, $n = 92$) than control conjugates (◇, $n = 98$) ($P < 0.001$). No significant difference was detectable for αTfR bead–Jurkat contact zones between C20:5-treated (◆, $n = 69$) and control (◇, $n = 52$) conjugates ($P > 0.05$). Asterisks in C indicate a significant difference ($P < 0.05$) of the mean GP values at the contact zones between αCD3- and αTfR-coated beads. Systemic changes in the lipidome: (**E**) comparing the double bond (db) composition of the PC species of 10 min, 37°C αCD3 and αTfR-immunoisolates and total lipids of Jurkat cells treated with 20:5 polyunsaturated fatty acid eicasopentanoic acid (C20:5) and untreated controls. Note in all membrane fractions the dramatically altered fatty-acid saturation profile of PC following C20:5 treatment; the enrichment of polyunsaturated (db ⩾5) PC species and the relative depletion in all membrane fractions of PC species with 1–4 unsaturations. Panel (**F**) depicts lipid class composition of membrane fractions prepared from C20:5-treated and control Jurkat cells. The mol% of the lipid classes was calculated as the sum of the mol% of all detected lipid species of the respective lipid class ($n = 3$ independent experiments, average estimate ± s.d.). No conclusions were made on differences between low abundant lipid classes (<1 mol%, inset).

Discussion

In this study, we have performed a global analysis of the molecular lipid composition of TCR activation domains in the T-cell plasma membrane. This analysis provides, for the first time, direct evidence for the lateral segregation of distinct lipid species into membrane domains during TCR activation.

Accumulation of Lo membrane-phase lipids at TCR signalling domains

A key feature of the αCD3 immunoisolated plasma membrane fragments, enriched in TCR signalling domains, is the accumulation of cholesterol, SM and saturated PC species. These lipid species support the formation of condensed Lo membrane phase in model membranes, and raft domains in cell membranes have been proposed to adopt properties akin to this Lo-phase (Brown and London, 1998; Veatch and Keller, 2003; Mukherjee and Maxfield, 2004; Simons and Vaz, 2004). Accumulation of lipid rafts at TCR activation plasma membrane domains is supported by biophysical data showing the condensation of the plasma membrane at these sites (Figure 5) (Gaus *et al*, 2005). Whether these phenomena reflect the coalescence of dynamic nanoscale resting state rafts or a *de novo* formation of raft-domains at TCR signalling sites cannot be ascertained with the methods used here.

αCD3 immunoisolated plasma membrane domains contain a significant amount of plasma membrane proteins not engaged in TCR signalling (Figure 1A). Thus, the characteristic lipid composition of the αCD3 immunoisolates is probably an underestimation of the enrichment of raft-forming molecular lipid species *in situ* at TCR signalling domain in the plasma membrane.

Stulnig *et al* (1998) reported that treatment of Jurkat cells with C20:5 fatty acids leads to inhibition of TCR activation and proposed that polyunsaturated lipid species disrupted the condensation of raft domains at TCR activation sites. Our lipidomic and the Laurdan data support this model. In a related approach, the incorporation of the oxysterol 7-ketocholesterol (7KC) into T cells was shown to impair the condensation of TCR activation sites. Indeed, 7KC is known to disturb the formation of liquid-ordered domains in model membranes (Massey and Pownall, 2005). As for the treatment with polyunsaturated C20:5, the 7KC incorporation resulted in an inhibition of T-cell activation (Rentero *et al*, 2008). These results suggest a functional link between TCR activation and plasma membrane lipid ordering at TCR activation sites. The coalescence of membrane rafts at TCR signalling sites could control signal transduction by modulating the rate and specificity of interacting signalling proteins, and/or by exclusion of unwanted interactors. However, this remains a model for future experiments. An alternative explanation involving the thickness of the membrane being defined by the transmembrane proteins occupying the different membrane domains should also be considered (Munro, 2003).

Direct loading of Jurkat cells with C20:5 polyunsaturated fatty acid altered the fatty acyl profile of all main glycerophospholipid species (Supplementary Figure S5) and disrupted the plasma membrane condensation at TCR activation site (Figure 5). This stands in contrast to the biochemical and biophysical alterations of T-cell plasma membranes from a dietary *n*-3 PUFA-exposed mouse (Fan *et al*, 2003; Kim *et al*, 2008). The T cells of PUFA-fed mice exhibited altered acyl chain saturation of PS and PE, whereas the saturation profile of PC and PI acyl chains were unaltered. As a further difference to the reduced membrane condensation following the acute PUFA-loading, a experimental regime mimicking a dietary PUFA exposure retained the specific condensation at T-cell activation sites (Kim *et al*, 2008). It is possible that these different outcomes of PUFA loading on T-cell rafts reflect the compensatory mechanisms that preserve the functions of T-cell membranes following the presentation of PUFA-rich diets.

The lipid bilayer of TCR signalling plasma membrane domains

Patches of antibody-cross-linked outer leaflet GPI-anchored proteins confine the movement/distribution of inner leaflet fatty acid-anchored raft proteins (Harder *et al*, 1998; Suzuki *et al*, 2007b). These observations indicate an interrelationship between the organization of lipids in the exoplasmic and the cytoplasmic leaflet at clustered raft domains in the plasma membrane. The nature of this connection represents an important open issue in membrane biology.

Analysis of PE, PS and PI species in Jurkat cells that are enriched in the inner plasma membrane leaflet (Zachowski, 1993; van Meer *et al*, 2008) showed that these lipid species in αCD3 immunoisolates (Figure 4) were predominantly unsaturated. However, the distinctive molecular composition of αCD3 immunoisolated plasma membrane fragments in comparison with the αTfR immunoisolated plasma membrane fragments is also reflected in these glycerophospholipids. We observed an enrichment of plasmenyl PE species (having a vinyl-ether-linked hydrocarbon moiety) as compared with total PE, and an enrichment of all PS species. We also detected a 3-fold reduction of the PI in the αCD3 immunoisolates. The causes for the PI depletion and the enrichment of plasmenyl PE species in the αCD3 isolates are currently unknown. Plasmenyl PE accumulation and PI depletion have been observed previously in a raft fraction separated from a crude plasma membrane fraction by a detergent-free method (Pike *et al*, 2002).

The molecular abundance of PS was significantly higher in αCD3 immunoisolates as compared with αTfR immunoisolates. It is interesting to note that the C20:5 treatment resulted in a reduction of the PS fraction in the αCD3 immunoisolates. The specific interactions of PS-rich membranes with the TCR–CD3 complex and the TCR signalling machinery have been reported in several studies. The TCR ζ-chain subunit changes its conformation upon binding to PS-rich membranes, possibly representing a regulatory event in the T-cell activation cascade (Aivazian and Stern, 2000). A similar charge-based interaction with anionic phospholipids was recently shown to determine a close contact and the conformation of cytoplasmic segment CD3ε with the inner leaflet of the T-cell plasma membrane (Xu *et al*, 2008). Phosphotyrosine-dependent reconstitution of LAT-nucleated signalling complexes on artificial lipid membranes *in vitro* readily occurred on membranes composed of PS but did not occur on phosphoLAT, which was anchored into liposomes composed of PC or PE (Sangani *et al*, 2009). Moreover, a specific recruitment of the protein kinase C isoform PKC θ and its activation at membrane surfaces enriched in PS was shown (Melowic *et al*, 2007). PKC θ is recruited to the immunological synapse and there it has an essential function

in the T-cell activation process (Altman and Villalba, 2003). These reports indicate that the PS accumulation at TCR signalling domains is most likely to represent a crucial element in the T-cell activation cascade.

The specific accumulation of distinct lipid species in TCR activation domains observed herein shows that it will be possible to directly analyse the lipidome of other signalling domains. Similar features as described for the molecular lipid composition of αCD3 isolates were reported for the HIV lipidome. Relative to the MT-4 host cell lipidome, HIV particles exhibited an increased concentration of SM, saturated PC, plasmenyl PE and PS species (Brugger *et al*, 2006). However, this study compared the HIV lipidome with the lipidome of the MT-4 host cell. Thus, this approach failed to resolve how the virus differed from the host cell plasma membrane from where it buds. A recent study by Chan *et al* (2008) confirmed the enrichment of Lo phase-forming lipids in the membrane of HIV, but additionally allowed relating the HIV lipidome to that of the plasma membrane isolated from host cells. This lipid analysis showed that cholesterol, ceramide and the ganglioside GM3 were higher in the virus as compared with the membrane from which the HIV envelope is derived. These studies represent the beginning of a new phase in lipid research. Until recently, it was not possible to perform lipidome-wide quantification of individual molecular lipid species from minute sample amounts. With new mass spectrometric methodology at hand, we can start to ascertain the functional implications of lipid complexity in biological membranes and their subdomains.

Materials and methods

Cell culture

Jurkat cells were maintained in RPMI medium with 10% FCS (BioSera), penicillin (100 μg/ml), streptomycin (100 U/ml) and 2 mM glutamax (all Gibco/BRL). Incorporation of the C20:5 polyunsaturated fatty acid at 50 μM in serum-free medium was described previously (Stulnig *et al*, 1998).

Antibodies and reagents

All common chemicals were purchased from Sigma Chemicals (St Louis, MO) and were of the best analytical grade. Solvents: water, methanol (both LiChrosolv® grade) and chloroform (LC grade) were from Merck (Darmstadt, Germany). Synthetic lipid standards were purchased from Avanti Polar Lipids, Inc. (Alabaster, AL). PI 17:0/17:0 was provided by Christoph Thiele (Max Planck Institute of Molecular Cell Biology and Genetics).

Mouse monoclonal antibodies against CD3 (OKT-3) and TfR (B3/25) were purified from tissue culture supernatant. We also used OKT-3 Ab and OKT-9 clone against CD71 (TfR) from eBioscience. Antibodies and reagents for western blotting were purchased from the following sources: LAT rabbit polyclonal antibody was obtained from Upstate Biotechnology; Calnexin polyclonal rabbit antibody was obtained from Sigma; MTCO1 mitochondrial marker antibody [1D6] was obtained from Abcam; TfR mouse monoclonal antibody was obtained from Zymed. Conjugated α-mouse IgG and α-rabbit IgG secondary antibodies and conjugated streptavidin were obtained from Bio-Rad or from LICOR Bioscience. M450 goat α-mouse Dynabeads were obtained from Invitrogen (London).

Western blotting

Precast 4–12% NuPAGE SDS gels were purchased from Invitrogen, and following electrophoresis the proteins were transferred to HybondC+ membranes (Amersham Bioscience) by semidry blotting using a Bio-Rad Trans-blot apparatus. Immunoreactive bands were visualized either by ECL chemiluminescence (Amersham Bioscience) or with infrared fluorescence detection using a LICOR Odysee detection system.

Immunoisolation

The immunoisolation of T-cell signalling domains was performed with minor alteration from the protocol reported previously (Harder and Kuhn, 2001). Goat α mouse dynabeads (M450) were coated with OKT-3 (αCD3) and B3/25 (αTfR) mAbs. Immunoisolates were prepared by incubating 5×10^7 Jurkat cells with 2.5×10^7 Dynabeads at 37°C for the indicated times and subsequent nitrogen cavitation at 50 bar for 10 min (Harder and Kuhn, 2001). Immunoisolates were washed three times in PBS and resuspended in 110 μl Millipore water. A quantity of 10 μl sample was removed for western blot analysis and the remaining sample was immediately frozen at −80°C.

Mass spectrometric lipid analysis

Total lipid extraction of Jurkat cells and immunoisolates was performed by a modified Bligh and Dyer method (Bligh and Dyer, 1959). The entire lipid extraction procedure was performed in 15 min at 4°C because the polystyrene beads are not resistant to chloroform. Samples (in 100 μl water) were thawed and 10 μl internal standard mixture was added, providing a total spike amount of 15 pmol DAG 17:0–17:0, 36 pmol PA 17:0–17:0, 78 pmol PE 17:0–17:0, 11 pmol PG 17:0–17:0, 64 pmol PS 17:0–17:0, 67 pmol PC 18:3–18:3, 82 pmol PI 17:0–17:0, 45 pmol SM 18:1;2/17:0;0, 15 pmol Cer 18:1;2/17:0;0, 30 pmol GalCer 18:1;2/12:0;0, 30 pmol LacCer 18:1;2/12:0;0, 61 pmol cholesterol-d7. Subsequently, 495 μl chloroform/methanol (2.5:1, v/v) was added and the samples were vigorously shaken for 15 min at 1400 r.p.m. on an Eppendorf ThermoMixer (Eppendorf, Hamburg, Germany). Samples were centrifuged for 2 min at 500 *g* to promote phase separation. The lower organic phase (total lipid extract) was isolated and evaporated in a vacuum exicator at 4°C. Total lipid extracts were dissolved in 50 μl chloroform/methanol (1:2, v/v) and subjected to quantitative lipid analysis on a hybrid QSTAR Pulsar *i* quadrupole time-of-flight mass spectrometer (MDS Sciex, Concord, Ontario, Canada) equipped with a robotic nanoflow ion source NanoMate HD System using a 4.1 μm nozzle diameter ESI-Chip (Advion Biosciences Inc., Ithaca, NJ). DAG, PA, PE, PS, PG and PI species were quantified by negative ion mode multiple PIS analysis (Ejsing *et al*, 2006): 15 μl total lipid extract was loaded in a polypropylene 96-well plate (Eppendorf, Hamburg, Germany) on top of 15 μl 0.01% (v/v) methylamine (in methanol), the 96-well plate was covered with aluminium foil and samples were infused in negative ion mode with ionization parameters of 0.5 psi and 0.9 kV. PC and SM were quantified by positive ion mode PIS *m/z* 184.1 analysis (Ekroos *et al*, 2002, 2003): 15 μl total lipid extract was loaded on top of 19.3 μl 13.3 mM ammonium acetate dissolved in 2-propanol, and samples were infused in positive ion mode with ionization parameters of 1.25 psi and 0.95 kV. Neutral sphingolipids were analysed after the PIS *m/z* 184.1 analysis using an additional period of multiple reaction monitoring with the target list: *m/z* 538.5 (Cer 18:1;2/16:0;0), *m/z* 552.5 (internal standard Cer 18:1;2/17:0;0), *m/z* 648.6 (Cer 18:1;2/24:1;0), *m/z* 650.6 (Cer 18:1;2/24:0;0), *m/z* 644.5 (internal standard GalCer = HexCer 18:1;2/12:0;0), *m/z* 700.6 (HexCer 18:1;2/16:0;0), *m/z* 810.7 (HexCer 18:1;2/24:1;0), *m/z* 812.7 (HexCer 18:1;2/24:0;0), *m/z* 806.6 (internal standard LacCer = Hex2Cer 18:1;2/12:0;0), *m/z* 862.6 (Hex2Cer 18:1;2/16:0;0), 972.7 (Hex2Cer 18:1;2/24:1;0), 974.7 (Hex2Cer 18:1;2/24:0;0). Cholesterol was quantified after chemical acetylation using multiple reaction monitoring as described previously (Liebisch *et al*, 2006). Automated processing of acquired spectra, identification and quantification of detected molecular lipid species was performed by Lipid Profiler software (MDS Sciex) as described previously (Ejsing *et al*, 2006).

Annotation of lipid species

Lipid species were annotated by their molecular composition or by their sum formula, depending on the mode of analysis. For sum formula annotations, the following convention was applied: ⟨lipid class⟩ ⟨total number of carbon atoms in the FA moieties⟩:⟨total number of double bonds in the FA moieties⟩ (e.g., PC 36:2). The molecular composition of glycerophospholipid species detected by multiple PIS was annotated as: ⟨lipid class⟩ ⟨number of carbon atoms in the first FA moiety⟩:⟨number of double bonds in the first FA moiety⟩−⟨number of carbon atoms in the second FA

moiety〉:〈number of double bonds in the second FA moiety〉 (e.g., PE 18:0–18:2). Ether species were annotated with the prefix *O*- (e.g., PC *O*-34:2 or PE *O*-16:1p–18:1).

Neutral sphingolipids were annotated by molecular composition: 〈lipid class〉 〈number of carbon atoms in the long-chain base moiety〉:〈number of double bonds in the long-chain base moiety〉;〈number of hydroxyl groups in the long-chain base moiety〉/〈number of carbon atoms in the fatty acid moiety〉:〈number of double bonds in the fatty acid moiety〉;〈number of hydroxyl groups in the fatty acid moiety〉. For example, the precursor ion at *m/z* 538.5 was identified as Cer 18:1;2/16:0;0, that is, a Cer species containing a C18 sphingosine (having two hydroxyl groups) and an C16 amide-linked fatty acid moiety with no double bonds or hydroxyl groups. Detected SM species were annotated by sum formula, as the PIS *m/z* 184.1 analysis does not provide structural information on the molecular composition of the long-chain base and amide-linked fatty-acid moiety. Detected SM species were annotated with the sum formula: SM 〈number of carbon atoms in the ceramide backbone〉:〈number of double bonds in the ceramide backbone〉;〈number of hydroxyl groups in the ceramide backbone〉. For example, the precursor ion at *m/z* 703.6 was identified as SM 34:1;2, that is, the SM species containing a total of 34 carbon atoms, one double bond and two hydroxyl groups in its ceramide backbone.

Microscopy

Jurkat cells were labelled with Laurdan (Gaus *et al*, 2005) by adding the dye (5 μM final concentration) to the serum-free media of C20:5 enrichment and incubating the cells for 30 min at 37°C. Cells were conjugated to beads and activates as for immunoisolation using polystyrene beads (SpheroTech). Cell–bead conjugates were allowed to settle on poly-L-lysine-coated glass coverslips and fixed in 4% paraformaldehyde. Laurdan fluorescence was excited at 800 nm with a Verdi/Mira 900 multi-photon laser system. Laurdan intensity images (Leica IRE3 microscope and software) were recorded simultaneously with emission in the range of 400–460 and 470–530 nm for the two channels, respectively. The relative sensitivity of the two channels was calibrated with 5 μM Laurdan in DMSO for each experiment. All images were recorded with a $\times 100$ oil objective, $N_A = 1.4$ at RT.

Image analysis

Laurdan intensity images were converted to GP images by calculating the normalized ratio of the two intensity channels, defined as

$$GP = \frac{I_{(400-460)} - I_{(470-530)}}{I_{(400-460)} + I_{(470-530)}}.$$

GP images were pseudo-coloured in Adobe Photoshop. To determine GP values at the contact sites, the mean GP area of the region of interest adjacent to the bead was determined. Each data point (or symbol) in the scatter plots represents one contact site. GP values were corrected using G-factor obtained for Laurdan in DMSO for each experiment (Gaus *et al*, 2003). Statistical comparisons were performed using one-way ANOVA with Tukey's multiple comparison test.

Supplementary data

Supplementary data are available at *The EMBO Journal* Online (http://www.embojournal.org).

Acknowledgements

We are grateful to Christoph Thiele (Max Planck Institute of Molecular Cell Biology and Genetics) for providing synthetic PI 17:0/17:0, Eva Duchoslav (MDS Sciex) for expert advice on Lipid Profiler software and Kim Ekroos (VTT Technical Research Centre of Finland) and Igor Chernushevich (MDS Sciex) for a long-standing collaboration in many aspects of QqTOF mass spectrometry. We thank Reinaldo Almeida and Mark Baumert (Advion Biosciences Inc.) for their expert advice on NanoMate HD System operation. We thank Oreste Acuto (University of Oxford) for making the LICOR Odysee system available to us. TZ and TH gratefully acknowledge the support by the EPA trust. The work in TH laboratory was supported by the Wellcome trust project grant 082782/2/07/2. This work was also supported by grants from the Deutsche Forschungsgemeinschaft to KS (SPP1175 and SFB-TR13) and AS (SFB-TR13). We thank Anton van der Merwe and Neil Barclay (both University of Oxford) for critically reading the manuscript.

References

Aivazian D, Stern LJ (2000) Phosphorylation of T cell receptor zeta is regulated by a lipid dependent folding transition. *Nat Struct Biol* **7:** 1023–1026

Altman A, Villalba M (2003) Protein kinase C-theta (PKCtheta): it's all about location, location, location. *Immunol Rev* **192:** 53–63

Bligh EG, Dyer WJ (1959) A rapid method of total lipid extraction and purification. *Can J Biochem Physiol* **37:** 911–917

Brown DA, London E (1997) Structure of detergent-resistant membrane domains: does phase separation occur in biological membranes? *Biochem Biophys Res Commun* **240:** 1–7

Brown DA, London E (1998) Structure and origin of ordered lipid domains in biological membranes. *J Membr Biol* **164:** 103–114

Brugger B, Glass B, Haberkant P, Leibrecht I, Wieland FT, Krausslich HG (2006) The HIV lipidome: a raft with an unusual composition. *Proc Natl Acad Sci USA* **103:** 2641–2646

Chan AC, Iwashima M, Turck CW, Weiss A (1992) ZAP-70: a 70 kd protein-tyrosine kinase that associates with the TCR zeta chain. *Cell* **71:** 649–662

Chan R, Uchil PD, Jin J, Shui G, Ott DE, Mothes W, Wenk MR (2008) Retroviruses human immunodeficiency virus and murine leukemia virus are enriched in phosphoinositides. *J Virol* **82:** 11228–11238

Douglass AD, Vale RD (2005) Single-molecule microscopy reveals plasma membrane microdomains created by protein–protein networks that exclude or trap signaling molecules in T cells. *Cell* **121:** 937–950

Ejsing CS, Duchoslav E, Sampaio J, Simons K, Bonner R, Thiele C, Ekroos K, Shevchenko A (2006) Automated identification and quantification of glycerophospholipid molecular species by multiple precursor ion scanning. *Anal Chem* **78:** 6202–6214

Ekroos K, Chernushevich IV, Simons K, Shevchenko A (2002) Quantitative profiling of phospholipids by multiple precursor ion scanning on a hybrid quadrupole time-of-flight mass spectrometer. *Anal Chem* **74:** 941–949

Ekroos K, Ejsing CS, Bahr U, Karas M, Simons K, Shevchenko A (2003) Charting molecular composition of phosphatidylcholines by fatty acid scanning and ion trap MS3 fragmentation. *J Lipid Res* **44:** 2181–2192

Fan YY, McMurray DN, Ly LH, Chapkin RS (2003) Dietary (n-3) polyunsaturated fatty acids remodel mouse T-cell lipid rafts. *J Nutr* **133:** 1913–1920

Gaus K, Chklovskaia E, Fazekas de St Groth B, Jessup W, Harder T (2005) Condensation of the plasma membrane at the site of T lymphocyte activation. *J Cell Biol* **171:** 121–131

Gaus K, Gratton E, Kable EP, Jones AS, Gelissen I, Kritharides L, Jessup W (2003) Visualizing lipid structure and raft domains in living cells with two-photon microscopy. *Proc Natl Acad Sci USA* **100:** 15554–15559

Gaus K, Zech T, Harder T (2006) Visualizing membrane microdomains by Laurdan 2-photon microscopy. *Mol Membr Biol* **23:** 41–48

Hancock JF (2006) Lipid rafts: contentious only from simplistic standpoints. *Nat Rev Mol Cell Biol* **7:** 456–462

Harder T (2004) Lipid raft domains and protein networks in T-cell receptor signal transduction. *Curr Opin Immunol* **16:** 353–359

Harder T, Kuhn M (2000) Selective accumulation of raft-associated membrane protein LAT in T cell receptor signaling assemblies. *J Cell Biol* **151:** 199–208

Harder T, Kuhn M (2001) Immunoisolation of TCR signaling complexes from Jurkat T leukemic cells. *Science's Signal Transduction*

Knowledge Environment. http://stkesciencemagorg/cgi/content/full/OC_sigtrans;2001/71/pl1

Harder T, Scheiffele P, Verkade P, Simons K (1998) Lipid domain structure of the plasma membrane revealed by patching of membrane components. *J Cell Biol* **141:** 929–942

Huppa JB, Davis MM (2003) T-cell-antigen recognition and the immunological synapse. *Nat Rev Immunol* **3:** 973–983

Ike H, Kosugi A, Kato A, Iino R, Hirano H, Fujiwara T, Ritchie K, Kusumi A (2003) Mechanism of Lck recruitment to the T-cell receptor cluster as studied by single-molecule-fluorescence video imaging. *Chemphyschem* **4:** 620–626

Kim W, Fan YY, Barhoumi R, Smith R, McMurray DN, Chapkin RS (2008) n-3 polyunsaturated fatty acids suppress the localization and activation of signaling proteins at the immunological synapse in murine CD4+ T cells by affecting lipid raft formation. *J Immunol* **181:** 6236–6243

Kuikka M, Ramstedt B, Ohvo-Rekila H, Tuuf J, Slotte JP (2001) Membrane properties of D-erythro-*N*-acyl sphingomyelins and their corresponding dihydro species. *Biophys J* **80:** 2327–2337

Liebisch G, Binder M, Schifferer R, Langmann T, Schulz B, Schmitz G (2006) High throughput quantification of cholesterol and cholesteryl ester by electrospray ionization tandem mass spectrometry (ESI-MS/MS). *Biochim Biophys Acta* **1761:** 121–128

Liebisch G, Lieser B, Rathenberg J, Drobnik W, Schmitz G (2004) High-throughput quantification of phosphatidylcholine and sphingomyelin by electrospray ionization tandem mass spectrometry coupled with isotope correction algorithm. *Biochim Biophys Acta* **1686:** 108–117

Massey JB, Pownall HJ (2005) The polar nature of 7-ketocholesterol determines its location within membrane domains and the kinetics of membrane microsolubilization by apolipoprotein A-I. *Biochemistry* **44:** 10423–10433

Melowic HR, Stahelin RV, Blatner NR, Tian W, Hayashi K, Altman A, Cho W (2007) Mechanism of diacylglycerol-induced membrane targeting and activation of protein kinase Ctheta. *J Biol Chem* **282:** 21467–21476

Mor A, Campi G, Du G, Zheng Y, Foster DA, Dustin ML, Philips MR (2007) The lymphocyte function-associated antigen-1 receptor costimulates plasma membrane Ras via phospholipase D2. *Nat Cell Biol* **9:** 713–719

Mukherjee S, Maxfield FR (2004) Membrane domains. *Annu Rev Cell Dev Biol* **20:** 839–866

Munro S (2003) Lipid rafts. Elusive or illusive? *Cell* **115:** 377–388

Pike LJ, Han X, Chung KN, Gross RW (2002) Lipid rafts are enriched in arachidonic acid and plasmenylethanolamine and their composition is independent of caveolin-1 expression: a quantitative electrospray ionization/mass spectrometric analysis. *Biochemistry* **41:** 2075–2088

Rentero C, Zech T, Quinn CM, Engelhardt K, Williamson D, Grewal T, Jessup W, Harder T, Gaus K (2008) Functional implications of plasma membrane condensation for T cell activation. *PLoS ONE* **3:** e2262

Sangani D, Vénien-Bryan C, Harder T (2009) Phosphotyrosine-dependent *in vitro* reconstitution of recombinant LAT-nucleated multiprotein signalling complexes on liposomes. *Mol Memb Biol* **26:** 1–13

Shaikh SR, Edidin M (2006) Polyunsaturated fatty acids, membrane organization, T cells, and antigen presentation. *Am J Clin Nutr* **84:** 1277–1289

Shaw AS (2006) Lipid rafts: now you see them, now you don't. *Nat Immunol* **7:** 1139–1142

Simons K, Toomre D (2000) Lipid rafts and signal transduction. *Nat Rev Mol Cell Biol* **1:** 31–39

Simons K, Vaz WL (2004) Model systems, lipid rafts, and cell membranes. *Annu Rev Biophys Biomol Struct* **33:** 269–295

Spitaler M, Emslie E, Wood CD, Cantrell D (2006) Diacylglycerol and protein kinase D localization during T lymphocyte activation. *Immunity* **24:** 535–546

Stulnig TM, Berger M, Sigmund T, Raederstorff D, Stockinger H, Waldhausl W (1998) Polyunsaturated fatty acids inhibit T cell signal transduction by modification of detergent-insoluble membrane domains. *J Cell Biol* **143:** 637–644

Suzuki KG, Fujiwara TK, Edidin M, Kusumi A (2007a) Dynamic recruitment of phospholipase C gamma at transiently immobilized GPI-anchored receptor clusters induces IP3-Ca2+ signaling: single-molecule tracking study 2. *J Cell Biol* **177:** 731–742

Suzuki KG, Fujiwara TK, Sanematsu F, Iino R, Edidin M, Kusumi A (2007b) GPI-anchored receptor clusters transiently recruit Lyn and G alpha for temporary cluster immobilization and Lyn activation: single-molecule tracking study 1. *J Cell Biol* **177:** 717–730

Tavano R, Contento RL, Baranda SJ, Soligo M, Tuosto L, Manes S, Viola A (2006) CD28 interaction with filamin-A controls lipid raft accumulation at the T-cell immunological synapse. *Nat Cell Biol* **8:** 1270–1276

van Meer G, Voelker DR, Feigenson GW (2008) Membrane lipids: where they are and how they behave. *Nat Rev Mol Cell Biol* **9:** 112–124

Veatch SL, Keller SL (2003) Separation of liquid phases in giant vesicles of ternary mixtures of phospholipids and cholesterol. *Biophys J* **85:** 3074–3083

Xu C, Gagnon E, Call ME, Schnell JR, Schwieters CD, Carman CV, Chou JJ, Wucherpfennig KW (2008) Regulation of T cell receptor activation by dynamic membrane binding of the CD3epsilon cytoplasmic tyrosine-based motif. *Cell* **135:** 702–713

Zachowski A (1993) Phospholipids in animal eukaryotic membranes: transverse asymmetry and movement. *Biochem J* **294** (Part 1)**:** 1–14

Zhang W, Sloan-Lancaster J, Kitchen J, Trible RP, Samelson LE (1998) LAT: the ZAP-70 tyrosine kinase substrate that links T cell receptor to cellular activation. *Cell* **92:** 83–92

